引用格式：ZHOU Dongmei, WANG Aihuan, LI Cuiran, et al. Design of Compact Polarization Beam Splitter Based on Triple-waveguide Directional Coupler[J]. Acta Photonica Sinica, 2022, 51(1):0151119
周冬梅,王爱环,李翠然,等. 基于三波导定向耦合器的紧凑型偏振分束器的设计[J].光子学报,2022,51(1):0151119

基于三波导定向耦合器的紧凑型偏振分束器的设计

周冬梅,王爱环,李翠然,吴小所,闫保万
(兰州交通大学 电子与信息工程学院,兰州 730070)

摘　要:为了提高偏振分束器的消光比,利用混合等离子体波导和条形介质波导之间的非对称定向耦合特性,设计了由两个尺寸不同的硅波导和一个中间输入混合等离子体波导组成的偏振分束器,采用三维时域有限差分法对偏振分束器的结构和性能进行优化。实验结果表明:混合等离子体波导中TE和TM模式的双折射率对比通过介质加载波导增强,可获得超紧凑的结构,实验耦合长度仅有4.6 μm;在1.55 μm的中心波长处,TE模式的偏振消光比为－38.9 dB,插入损耗为0.5 dB,TM模式的消光比为－34.7 dB,插入损耗为0.45 dB,设计的偏振分束器具有高消光比;在波导制作公差范围内,模式的插入损耗小于2.8 dB,消光比低于－22.5 dB。

关键词:集成光学器件;偏振分束器;时域有限差分法;光波导;消光比;插入损耗
中图分类号:TN256　　**文献标识码**:A　　**doi**:10.3788/gzxb20225101.0151119

0　引言

近年来,绝缘体上硅(Silicon-on-Insulator,SOI)与互补金属氧化物(Complementary Metal-oxide Semiconductor,CMOS)工艺具有兼容和易于集成的优点,吸引了人们对实现紧凑光子集成电路的大量关注[1,2]。然而,由于SOI波导中硅和二氧化硅之间的高折射率差经常会引入强烈的偏振依赖性,使TE和TM模式在SOI波导中具有不同的传播特性[3],可能会干扰光互连和量子通信中的光信号。为了解决这个问题,提出了偏振旋转器(Polarization Rotator,PR)[4,5]、偏振分束器(Polarization Beam Splitter,PBS)[6,7]和偏振分束转换器(Polarization Splitter-Rotator,PSR)[8,9]等设备。其中,PBS分离/组合两种正交偏振模式,避免了光通信中的模式干扰问题。

目前,报道了各种波导结构来实现片上PBS,例如定向耦合器(Directional Coupler,DC)[10,11]、多模干涉仪(Multimode Interferometer,MMI)[12,13]、马赫-曾德干涉仪(Mach-Zehnder Interferometer,MZI)[14]和亚波长光栅(Subwavelength-Grating,SWG)[15-17]结构等。在这些结构中,基于DC的PBS由于其优越的性能和简单的设计而受到关注,尤其是基于非对称DC(Asymmetrical Directional Coupler,ADC)的PBS依赖多个不同的波导,增强TE和TM模式之间的折射率对比,有效地实现高消光比和小占地面积。CHEN D等[18,19]提出了由两个平行的SOI条形波导组成的PBS,其结构简单易于实现,但该器件的耦合长度较长,导致器件整体占地面积大。FENG J等[3,20]利用狭缝波导结构ADC减小耦合长度,通过将模式限制在不同的波导区域获得较小的占地面积,但是该器件的消光比(Extinction Ratio,ER)不足,并且刻蚀产生的狭缝波导侧壁粗糙带来的散射损耗也会影响器件的性能。DAI D X等[21,22]提出了基于弯曲DC的PBS实现了超小尺寸和高制造容

基金项目:国家自然科学基金(Nos.61661025, 62161016)
第一作者:周冬梅(1975—),女,副教授,硕士,主要研究方向为光传输技术、无线移动通信技术、人工智能技术在通信领域的应用等。Email: 912506338@qq.com
导师(通讯作者):李翠然(1975—),女,教授,博士,主要研究方向为无线通信技术、认知无线电技术、移动自组网技术等。Email: 2373416425@qq.com
收稿日期:2021-08-16;**录用日期**:2021-09-24

差，但由于DC中有一些不希望的残余交叉耦合，TE偏振的ER还是不高。

硅作为介质材料的混合等离子体波导（Hybrid Plasmonic Waveguide，HPW）具有传播长度长和约束强的优势[23]。HPW由高折射率电介层（如Si）、金属帽（如Ag）以及中间的低折射率间隔物（如SiO_2）构成。相比较传统的介质波导，HPW有显著的双折射效应[24]，其巨大的偏振多样性使得TE和TM能够在两个不同的层中传输，有望突破光子器件尺寸的限制[25]，并且与SOI技术兼容，提供了在同一平台上集成硅光子学和等离子体的可能。因此，为了提高消光比和减小器件尺寸，本文提出了一种基于ADC的混合等离子体辅助的PBS，该器件由SOI平台上两个尺寸不同的硅波导和一个中间输入HPW组成，两侧的硅基波导通过相位匹配条件将HPW中的TE和TM模式分别耦合分离。

1 器件结构与设计

为了实现ADC结构的水平和垂直不对称，一种简单的方法是为耦合区域选择不同的波导类型，为上包层和下包层选择不同的材料。本文提出的基于混合等离子体波导的PBS的立体结构和耦合区域横截面示意图如图1所示。该器件是由在SOI晶片上的两个Si波导和中间输入波导组成。输入波导是一种混合表面等离子体波导，选择Si、SiO_2和Ag作为模拟材料；而两侧的耦合输出波导选择高度不同的Si材料，分别用于耦合TM和TE模式。上下包层分别选择为空气和SiO_2来打破垂直对称性。输入波导、TE模式耦合波导和TM模式耦合波导的Si层厚度分别表示为h_1、h_2和h_3，三个波导的宽度分别表示为W_{in}、W_{TE}和W_{TM}。TE和TM偏振的耦合长度分别表示L_{c1}和L_{c2}。在该器件设计中，必须确保输入波导和TM耦合波导在TM模式下相位匹配，但在TE模式中相位不匹配。在TE耦合波导的情况下，反之亦然。与单模耦合结构相比，该结构通过双模耦合提高PBS的偏振消光比，此外，它还削弱了TE和TM模式对中间波导的依赖性[26]。

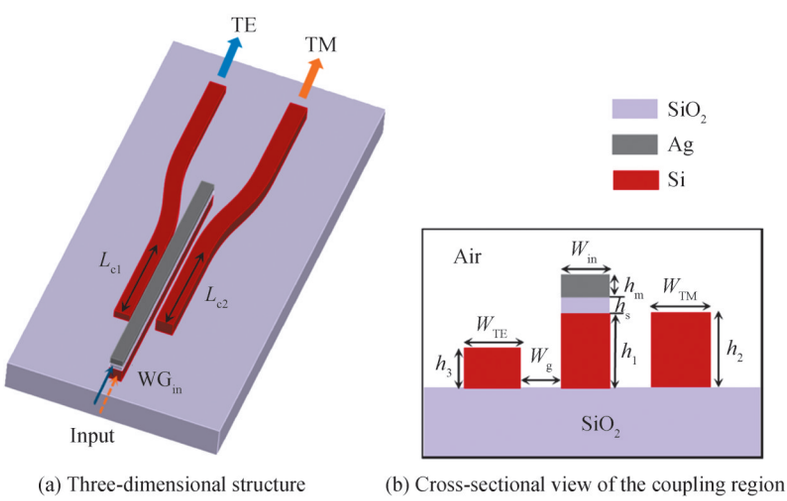

图1 PBS结构示意图

Fig.1 Schematic diagram of PBS structure

在该设计中，HPW的硅层厚度h_1为0.34 μm，TM耦合波导高度h_2与HPW中h_1一样，h_2=0.34 μm。为了保证TE耦合波导中的TM模式截止，设计了一个具有不同硅厚度的TE耦合波导，h_3选择为0.18 μm。图2显示了在1 550 nm波长下不同厚度的SiO_2夹层中TE与TM模式有效折射率的变化，从附图中可以看出，TM模式集中在SiO_2夹层中传输，而TE模式集中在Si波导中传输，因此，TM模式的有效折射率对SiO_2厚度的变化比较敏感。当SiO_2夹层的厚度比较大时，模式被很好地约束在SiO_2夹层和Si波导中传输，金属层对模场几乎没有影响；然而，当SiO_2夹层的厚度小于50 nm时，金属层会对TM偏振模式的场分布产生明显的影响。此外，还考虑到SiO2夹层厚度的选取对波导损耗有影响，则hs折中选择为50 nm。金属帽Ag的厚度hm为100 nm。在1 550 nm的波长下，Si、SiO2和Ag的有效折射率分别为neffsi=3.455，neffSiO_2=1.445，neffAg=0.1453+11.3587i[27]。

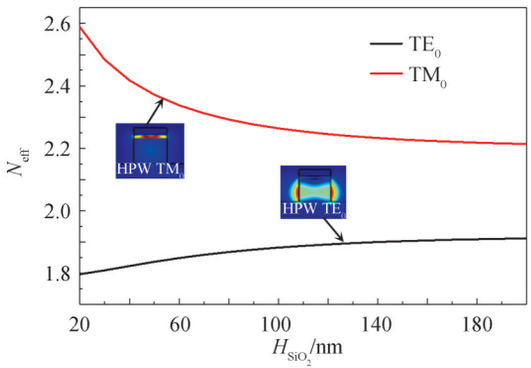

图2 基模有效折射率随SiO_2夹层厚度的变化,插图显示了在输入HPW中两种基模的电场分量

Fig.2 Effective indices of the fundamental modes vary with the thickness of the SiO_2 interlayer. The insets show the electrical field profiles of the two fundamental modes in the input HPW

当耦合区域中两个平行波导间距较大时,模式光信号各自独立地在其相应的波导中传输,此时在耦合区域的平行波导之间没有发生模式耦合。两个平行波导相互靠近,组成一个耦合系统。当波导之间的距离接近波长量级,由于倏逝波的作用,相邻两条平行波导的光信号会发生能量转换,即平行波导之间发生了倏逝波耦合。尤其当输入HPW中的某一偏振模式与耦合波导中某一模式的有效折射率相等,即满足相位匹配条件,能精确地激发耦合波导中特定的模式,通过选取优化的耦合长度,可以将HPW中信号的能量完全转换到另一个波导中。根据耦合模理论,通过选取合适的三波导结构参数使得在模式耦合过程中某一个模式匹配而另一个模式失配,使用三维时域有限差分(3D Finite Difference Time Domain, 3D-FDTD)方法进行模式求解,优化HPW和TE/TM模式耦合波导的宽度和耦合长度。当Si波导的宽度低于0.4 μm时,它是单模波导,则输入波导宽度选择为W_{in}=0.3 μm。图3通过使用有限元法(Finite Element Method,FEM)计算了在1 550 nm波长下,HPW中TM和TE模式、TE耦合波导中TE模式和TM耦合波导中TM模式的有效折射率随各自波导宽度的变化。为了使HPW与TE耦合波导之间耦合TE模式,需要确保两个波导中n_{effTE}值非常相近,且n_{effTM}值相差比较大。由图3根据相位匹配条件,得出TE耦合波导的匹配宽度为W_{TE}=0.38 μm。同理,为了HPW与TM耦合波导之间耦合TM模式,得出TM耦合波导的相位匹配宽度为W_{TM}=0.416 μm。HPW与耦合波导之间的间隙越窄,波导的耦合长度就越短,器件尺寸就越紧凑[28],但考虑到工艺制造的困难,ADC的两个波导之间的间隙不能太窄[29]。在该设计中,两个相邻波导之间的间隙宽度选择为W_g=150 nm。

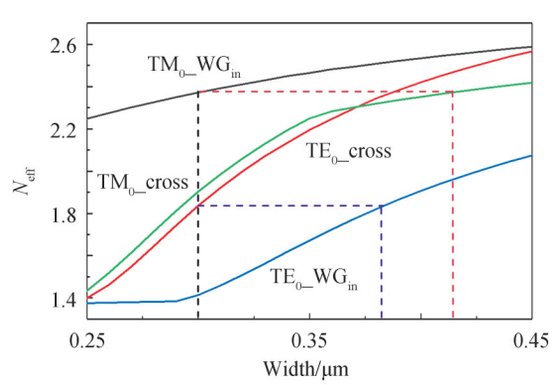

图3 HPW和TE/TM交叉波导中基模的有效折射率随各自波导宽度的变化

Fig.3 The effective indices of the fundamental modes in HPW and TE/TM-cross waveguides vary with the width of their waveguides

为了使HPW中预期的模式完全耦合到各自的耦合波导中,不仅需要HPW与耦合波导的宽度满足相位匹配条件,还需要选取最优的耦合长度。使用3D-FDTD方法计算ADC中HPW与TE/TM耦合波导的耦合长度的优化设计。决定PBS性能的关键参数是偏振转换效率(Polarization Conversion Efficiency,PCE),

对于TE和TM模式的PCE定义为

$$E_{\mathrm{TM}}=T_{\mathrm{TM\_cross}}/(T_{\mathrm{TM\_cross}}+T_{\mathrm{TE\_cross}}) \tag{1}$$

$$E_{\mathrm{TE}}=T_{\mathrm{TE\_cross}}/(T_{\mathrm{TE\_cross}}+T_{\mathrm{TM\_cross}}) \tag{2}$$

式中，$T_{\mathrm{TM_cross}}$和$T_{\mathrm{TE_cross}}$分别表示TM和TE模式分别在TM耦合端口和TE耦合端口输出的透射率。图4展示了该PBS的HPW中输入TE和TM模式的PCE随耦合长度的变化。对于TE模式，当耦合长度为4.2 μm时，PCE可以达到0.947；对于TM模式，当耦合长度为4.6 μm时，PCE可以达到0.958。为了获得高的PCE，TE和TM模式耦合器的最佳耦合长度分别选择为L_{c1}=4.2 μm，L_{c2}=4.6 μm。

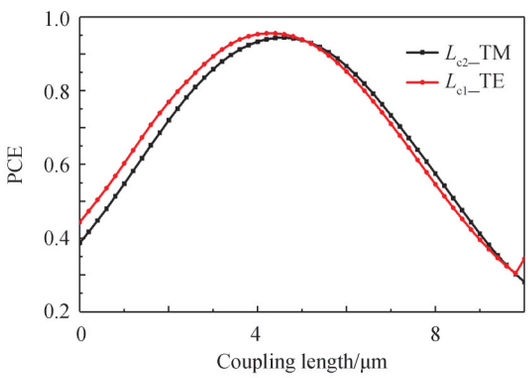

图4 HPW中TE和TM模式的偏振转换效率随耦合长度的变化

Fig.4 The polarization conversion efficiency of TE and TM modes in HPW as a function of coupling length

2 器件的性能分析

对于设计的PBS，使用具有非均匀网格尺寸的三维时域有限差分(3D-FDTD)法来研究模式特性。图5为所设计PBS在1550 nm波长下HPW中TE和TM模式耦合到TE/TM耦合波导的光场传输图。从图5(a)～(b)可以看出，当HPW中TE偏振光发射到输入端口时，在截面①，TE模式大部分集中在HPW的硅层中；在截面②，TE模式传输至耦合区域，有一部分光正在从HPW耦合到TE耦合波导；在截面③，几乎所有的光场都已经交叉耦合到TE耦合波导中，几乎没有任何模式混合。同理，从图5(c)～(d)看出，当HPW中

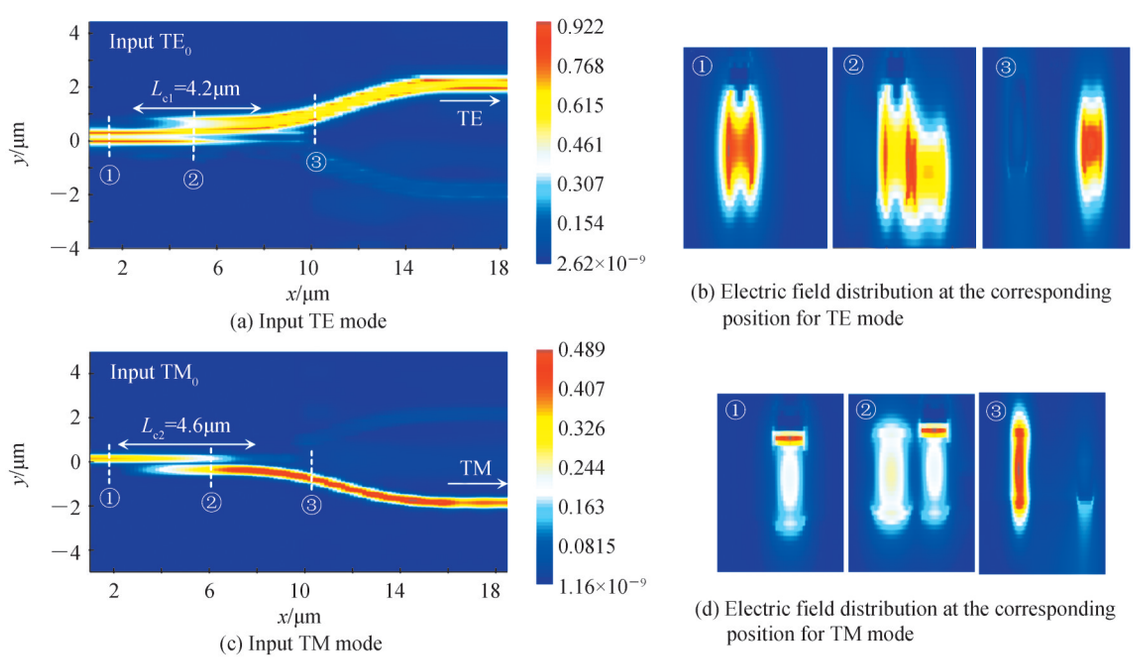

图5 PBS中的光场传输

Fig. 5 Light propagation of PBS

输入TM偏振模式时,在截面①,TM模式在HPW中高度集中在低折射率间隔层SiO_2中;传输至截面②时,有一大部分光正在从HPW耦合进TM耦合波导;在截面③,几乎所有的光场都已经耦合到TM耦合波导中,实现了光场能量从输入HPW完全耦合到相邻波导中。在整个器件的设计中,PBS的性能主要由偏振消光比(Polarization Extinction Ratio,PER)和插入损耗(Insertion Loss,IL)来评估,其定义为

$$R_{TM}=10\log_{10}(P_{TE}/P_{TM}) \tag{3}$$

$$R_{TE}=10\log_{10}(P_{TM}/P_{TE}) \tag{4}$$

$$L_{TE}=10\log_{10}(P_{TE}/P_{Input\_TE}) \tag{5}$$

$$L_{TM}=10\log_{10}(P_{TM}/P_{Input\_TM}) \tag{6}$$

式中,P_{TM}是耦合端口处TM模式的功率,P_{TE}是耦合端口处TE模式的功率,P_{Input_TE}和P_{Input_TM}分别为输入端口处TE和TM模式的功率。

图6显示了不同波长下TE和TM模式的PER和IL的变化。当输入TE模式时,在1.55 μm中心波长处,PER的值为−38.9 dB,IL的值为0.5 dB。对于1.48~1.62 μm的带宽内,TE模式的IL小于0.92 dB,由于在TE耦合波导中存在一小部分TM模式,则PER低于−28.3 dB。当输入TM模式时,在1.55 μm波长处,PER的值为−34.7 dB,IL的值为0.45 dB。在以1.55 μm为中心的140 nm的大波段内,TM模式的IL小于0.89 dB,PER低于−34.6 dB。这意味着PBS性能对波长不敏感。

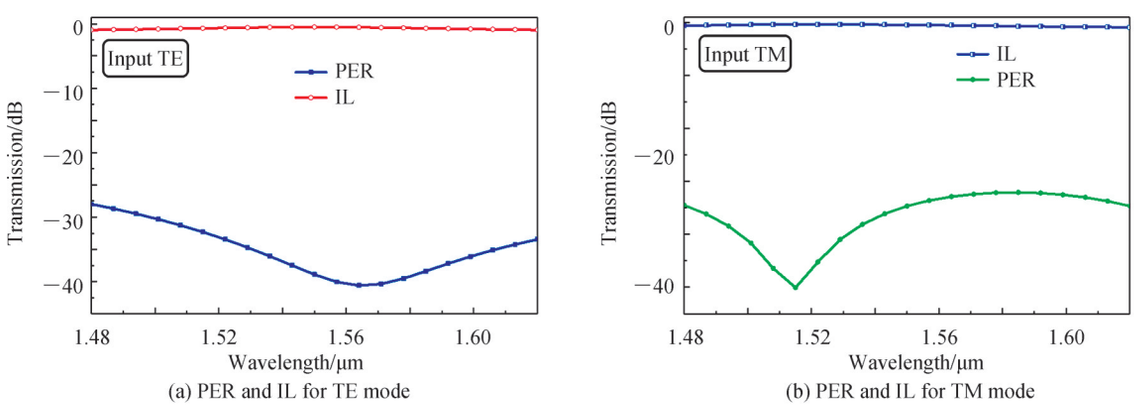

图6 TE和TM模式的透射率随波长的变化

Fig. 6 Wavelength dependence of transmission for both TE and TM modes

在该器件中,TM耦合波导的厚度为0.34 μm,而TE耦合波导的厚度为0.18 μm,不利于集成到平面电路中。因此,在分束结束时,TE耦合波导中的模式需要传输到厚度为0.34 μm的硅波导。图7为TE模式在波导厚度从0.18 μm突变到0.34 μm的电场分布,可以看出,模式在传输过程中基本不受影响。经过计算得出,TE模式在厚度变化的传输过程中传输损耗小于0.9 dB,意味着波导厚度的突变对器件整体性能的影响不大。

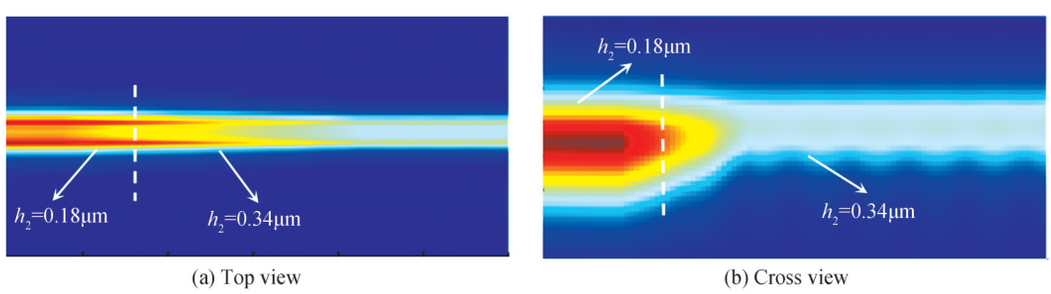

图7 波导厚度变化时TE模式的电场分布

Fig. 7 The electric field distribution for the TE mode when the thickness of the waveguide changes

工艺设计流程：首先使用具有340 nm厚顶部硅层和2 μm厚掩埋二氧化硅的标准SOI晶片，通过利用电子束光刻技术来转移结构图案；随后利用感应耦合等离子体刻蚀工艺对硅芯层进行刻蚀得到中间硅波导和TE/TM耦合波导；接着采用等离子体增强化学气相沉积工艺，在该结构的中间波导上沉积50 nm厚的SiO_2纳米层薄膜，最后进行100 nm厚金属层Ag的沉积和剥离，形成所提出的PBS。该器件在实际制造过程中不可避免地存在一定的尺寸变化，从而影响器件性能，本文选择在±20 nm波导宽度和±5 nm波导厚度公差范围内评估工艺容差。PBS的三个波导的宽度误差ΔW（$W_{in}=W_{in}+\Delta W$，$W_{TE}=W_{TE}+\Delta W$，$W_{TM}=W_{TM}+\Delta W$，$W_g=W_g-\Delta W$）从－20 nm到＋20 nm等间隔10 nm变化，Si波导厚度误差Δh（$h_1=h_1+\Delta h$，$h_2=h_2+\Delta h$，$h_3=h_3+\Delta h$）和SiO_2波导厚度误差Δh_s（$h_s=h_s+\Delta h_s$）从－5 nm到＋5 nm等间隔5 nm变化。由于Ag金属层对模场分布几乎没有影响，在工艺容差评估过程中不再讨论其对模式损耗和消光比的影响。图8为设计的PBS中输入TE/TM模式的PER和IL在不同波导宽度和厚度偏差的变化，可以看出，当波导的宽度和厚度远离初始值时，每个曲线获得了不同的波动变化。在±20 nm波导宽度的容差范围内，当输入TE模式时，TE模式的IL小于1.86 dB，PER低于－23.5 dB；当输入TM模式时，TM模式的IL小于2.3 dB，PER低

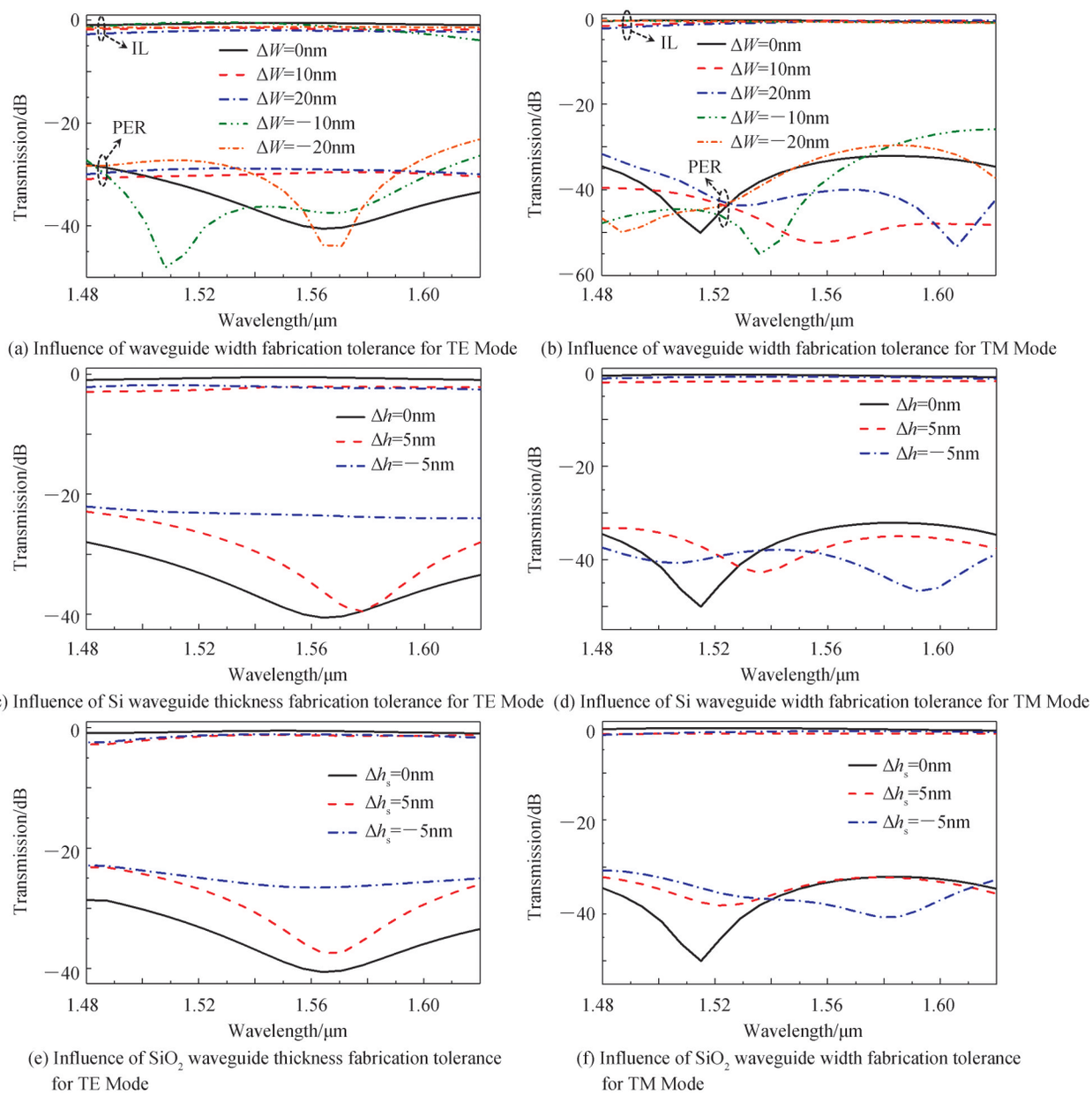

(a) Influence of waveguide width fabrication tolerance for TE Mode

(b) Influence of waveguide width fabrication tolerance for TM Mode

(c) Influence of Si waveguide thickness fabrication tolerance for TE Mode

(d) Influence of Si waveguide width fabrication tolerance for TM Mode

(e) Influence of SiO_2 waveguide thickness fabrication tolerance for TE Mode

(f) Influence of SiO_2 waveguide width fabrication tolerance for TM Mode

图8 TE和TM模式的PER和IL在工艺容差范围内的变化

Fig. 8 Variations of PER and IL in different fabrication tolerance for TE and TM modes

于－26.1 dB。在±5 nm Si波导厚度的容差范围内,模式的IL保持小于2.8 dB,PER低于－22.8 dB。在±5 nm SiO_2波导厚度的容差范围内,模式的IL保持小于2.7 dB,PER低于－22.5 dB。因此,该器件具有相当大的制作容差,且在容差范围内,器件的性能良好。

表1为本文中基于混合等离子体波导DC的PBS与基于硅基波导DC的PBS之间的PER、IL和耦合长度几个参数之间的性能比较。从表1中可以看出,与报道的基于DC的PBS相比[26, 30-34],本文提出的PBS具有较高的PER和宽的工作带宽,且耦合长度仅为4.6 μm,有效缩小了占地面积。

表1　基于DC实现不同结构PBS的性能比较

Table 1　The performance comparison of PBS with different structures based on DC

Reference	Structure	PER/dB	IL/dB	Bandwidth/nm	Coupling length/μm
[30]	Straight DC	<－20	0.5	1 540～1 570	19
[31]	Bent DC	<－20	～1	1 520～1 600	22.5
[32]	Triple Bent DC	<－30	<2	1 520～1 610	13
[33]	Triple straight DC	<－15	<0.5	1 510～1 570	17.7
[34]	Triple straight DC	<－20	<0.35	1 500～1 600	7.67
[26]	Triple straight DC	<－18	<0.3	1 500～1 600	9.9
This work (theoretical)	Triple straight DC	<－28.3	<0.92	1 480～1 620	4.6

3　结论

本文提出了一种基于三波导ADC的混合等离子体辅助的PBS,其具有紧凑的结构和宽带工作特性的优点。输入HPW和两个耦合输出的硅波导的尺寸已经优化,以便于将输入的TE和TM模式分别耦合进各自耦合波导中,从而发生偏振分离。采用3D-FDTD来研究模式特性并对器件性能进行分析。在该设计中,对于TE和TM模式的耦合长度分别为4.2 μm和4.6 μm,模式的PCE可以达到94.7%以上。在1.55 μm的工作波长,TE模式的PER可以达到－38.9 dB,IL小于0.5 dB;而对TM模式,PER值为－34.7 dB,IL值小于0.45 dB。在100 nm的工作带宽内,TE模式的消光小于－31.4 dB,TM模式的消光比小于－32.2 dB。此外,分析了PBS中三个波导的制造容差范围内的PER和IL,结果表明该器件具有较高的制造容差。相比传统的PBS,该基于三波导的PBS实现了双模耦合,具有超紧凑结构、高消光比和宽工作带宽的优点,在硅基光子集成电路中具有潜在的应用,可以为下一代光或量子通信带来新的希望。

参考文献

[1] GAO L, HU F, WANG X, et al. Ultracompact and silicon-on-insulator-compatible polarization splitter based on asymmetric plasmonic - dielectric coupling[J]. Applied Physics B, 2013, 113(2): 199-203.

[2] XIANG Tong, CHEN Heming, HU Yuchen, et al. Silicon-based integrated device for electro-optic modulation assembly with mode-division multiplexing[J]. Chinese Journal of Laser, 2021, 48(11): 1106001.
项彤, 陈鹤鸣, 胡宇宸, 等. 硅基电光调制与模分复用集成器件[J]. 中国激光, 2021, 48(11): 1106001.

[3] FENG J, AKIMOTO R, ZENG H. Asymmetric silicon slot-waveguide-assisted polarizing beam splitter [J]. IEEE Photonics Technology Letters, 2016, 28(12): 1294-1297.

[4] CHEN D, XIAO X, WANG L, et al. Highly efficient silicon optical polarization rotators based on mode order conversions [J]. Optics Letters, 2016, 41(5): 1070-1073.

[5] GALLACHER K, MILLAR R W, GRIŠKEVIČIŪTĖ U, et al. Ultra-broadband mid-infrared Ge-on-Si waveguide polarization rotator[J]. APL Photonics, 2020, 5(2): 1-7.

[6] SUN C, YU Y, DING Y, et al. Integrated mode-transparent polarization beam splitter supporting thirteen data channels [J]. Photonics Research, 2020, 8(6): 978-985.

[7] CHEN W, ZHANG B, WANG P, et al. Ultra-compact and low-loss silicon polarization beam splitter using a particle-swarm-optimized counter-tapered coupler[J]. Optics Express, 2020, 28(21): 30701-30709.

[8] CHEN D, LIU M, ZHANG Y, et al. C + L band polarization rotator-splitter based on a compact S-bend waveguide mode demultiplexer[J]. Optics Express, 2021, 29(7): 10949-10957.

[9] YIN Y, LI Z, DAI D. Ultra-broadband polarization splitter-rotator based on the mode evolution in a dual-core adiabatic taper[J]. Journal of Lightwave Technology, 2017, 35(11): 2227-2233.

[10] LI C, DAI D J O L. Compact polarization beam splitter for silicon photonic integrated circuits with a 340-nm-thick silicon core layer[J]. Optics Letters, 2017, 42(21): 4243-4246.

[11] KIM D W, LEE M H, KIM Y, et al. Planar-type polarization beam splitter based on a bridged silicon waveguide coupler [J]. Optics Express, 2015, 23(2): 998-1004.
[12] GUAN X, WU H, SHI Y, et al. Extremely small polarization beam splitter based on a multimode interference coupler with a silicon hybrid plasmonic waveguide [J]. Optics Letters, 2014, 39(2): 259-262.
[13] XU L, WANG Y, KUMAR A, et al. Polarization beam splitter based on MMI coupler with SWG birefringence engineering on SOI[J]. IEEE Photonics Technology Letters, 2018, 30(4): 403-406.
[14] AHMMED K T, CHAN H P, LI B. Three-mode multiplexer and demultiplexer based on the Mach-Zehnder interferometer[C]. OSA Continuum, 2021, 4(5): 1519-1532.
[15] GUO Chucai, YE Weimin, YUAN Xiaodong, et al. Research on sub-wavelength grating polarizing beam splitter[J]. Acta Optica Sinica, 2010, 30(9): 2690-2695.
郭楚才, 叶卫民, 袁晓东, 等. 亚波长光栅偏振分束器的研究[J]. 光学学报, 2010, 30(9): 2690-2695.
[16] CHENG Z, WANG J, YANG Z, et al. Sub-wavelength grating assisted mode order converter on the SOI substrate[J]. Optics Express, 2019, 27(23): 34434-34441.
[17] YANG Jiangtao WANG Jianan, WANG Yin, et al. Sub-wavelength metal-grating polarizer fabricated on a flexible substrate[J]. Chinese Journal of Lasers, 2020, 47(11): 1113004.
杨江涛, 王健安, 王银, 等. 基于柔性材料的亚波长金属光栅偏振器的关键技术研究[J]. 中国激光, 2020, 47(11): 1113004.
[18] CHEN D, XIAO X, WANG L, et al. Broadband, fabrication-tolerant polarization beam splitters based on a tapered directional coupler[J]. IEEE Photonics Technology Letters, 2016, 28(19): 2074-2077.
[19] LIN S, HU J, CROZIER K B. Ultracompact, broadband slot waveguide polarization splitter[J]. Applied Physics Letters, 2011, 98(15): 1-3.
[20] LIU Y, CHANG L, LI Z, et al. Polarization beam splitter based on a silicon nitride-silica-silicon horizontal slot waveguide[J]. Optics Letters, 2019, 44(6): 1335-1338.
[21] DAI D X, BOWERS J E. Novel ultra-short and ultra-broadband polarization beam splitter based on a bent directional coupler[J]. Optics Express, 2011, 19(19): 18614-18620.
[22] WU H, TAN Y, DAI D. Ultra-broadband high-performance polarizing beam splitter on silicon[J]. Optics Express, 2017, 25(6): 6069-6075.
[23] HU T, QIU H, ZHANG Z, et al. A compact ultrabroadband polarization beam splitter utilizing a hybrid plasmonic Y-branch[J]. IEEE Photonics Journal, 2016, 9(14): 4802209.
[24] GUAN X, WU H, SHI Y, et al. Ultracompact and broadband polarization beam splitter utilizing the evanescent coupling between a hybrid plasmonic waveguide and a silicon nanowire[J]. Optics Letters, 2013, 38(16): 3005-3008.
[25] CHANG K W, HUANG C C. Ultrashort broadband polarization beam splitter based on a combined hybrid plasmonic waveguide[J]. Scientific Reports, 2016, 6(1): 19609.
[26] NIU C Q, LIU Z, LI X L, et al. High extinction ratio polarization beam splitter realized by separately coupling[J]. IEEE Photonics Technology Letters, 2020, 32(18): 1183-1186.
[27] XU Y, XIAO J, SUN X. Proposal for compact polarization splitter using asymmetrical three-guide directional coupler[J]. IEEE Photonics Technology Letters, 2015, 27(6): 654-657.
[28] JIANG W, MIAO J, LI T. Compact silicon 10-mode multi/demultiplexer for hybrid mode- and polarization-division multiplexing system[J]. Scientific Reports, 2019, 9(1): 13223.
[29] XIAO R, SHI Y, LI J, et al. Integrated Bragg grating filter with reflection light dropped via two mode conversions[J]. Journal of Lightwave Technology, 2019, 37(9): 1946-1953.
[30] GUAN H, NOVACK A, STRESHINSKY M, et al. CMOS-compatible highly efficient polarization splitter and rotator based on a double-etched directional coupler[J]. Optics Express, 2014, 22(3): 2489-2496.
[31] CHEN S, WU H, DAI D. High extinction-ratio compact polarization beam splitter on silicon[J]. Electronics Letters, 2016, 52(12): 1043-1045.
[32] ONG J R, ANG T Y, SAHIN E, et al. Broadband silicon polarization beam splitter with a high extinction ratio using a triple-bent-waveguide directional coupler [J]. Optics Letters, 2017, 42(21):4450-4453.
[33] LI C, DAI D. Compact polarization beam splitter based on a three-waveguide asymmetric coupler with a 340-nm-thick silicon core layer[J]. Journal of Lightwave Technology, 2018, 36(11): 2129-2134.
[34] CHENG Z, WANG J, HUANG Y, et al. Realization of a compact broadband polarization beam splitter using the three-waveguide coupler[J]. IEEE Photonics Technology Letters, 2019, 31(22): 1807-1810.

Design of Compact Polarization Beam Splitter Based on Triple-waveguide Directional Coupler

ZHOU Dongmei, WANG Aihuan, LI Cuiran, WU Xiaosuo, YAN Baowan
(*School of Electronic and Information Engineering, Lanzhou Jiaotong University, Lanzhou* 730070, *China*)

Abstract: In recent years, the silicon-on-insulator platform has attracted much interest in implementing integrated optical circuits. Due to the high refractive index contrast between the waveguide and cladding, the silicon-on-insulator waveguide has a strong light confinement ability, which helps the device to achieve a compact structure size and large-scale integration. However, this high refractive index contrast causes silicon nanophotonic devices to have high polarization sensitivity so that TE and TM modes have different propagation characteristics in an identical silicon-on-insulator waveguide, which may disrupt the optical signals in optical interconnections and quantum communications. To tackle this problem, one solution is using a polarization beam splitter to polarize the TM mode and TE mode light. Considering future ultra-dense photonic integrated circuits, a compact PBS with high performance is desired. Therefore, the hybrid plasma waveguide is introduced into the design of the polarization beam splitter. The hybrid plasmonic waveguide consists of a high refractive index dielectric layer (e.g., Si), a metal cap (e.g., Ag), and a thin low-index material layer (e. g., SiO_2) between the Si layer and the metal layer. Compared with the traditional dielectric waveguide, it has a significant birefringence effect, which can maintain the performance of the device and further reduce the size of the device.In this paper, we propose and optimize a novel hybrid plasmonic polarization beam splitter utilizing asymmetrical directional coupling between the dielectric waveguides and a hybrid plasmonic waveguide on the silicon-on-insulator platform, which is ultracompact, and low-loss. Employing phase-matching conditions and super-mode theory, this polarization beam splitter is elaborately designed. The device is a three-waveguide asymmetric directional coupler. The middle hybrid plasmonic waveguide, which has a dielectric-loaded structure to enhance the refractive index contrast, is defined as the input waveguide. And different silicon-based waveguides on both sides are used to couple and separate TE and TM modes. Compared with the traditional polarization beam splitter based on the directional coupler composed of the same waveguide, this device facilitates two different types of waveguides to enhance the structural birefringence, which provides the device with an ultra-short coupling length and high extinction ratio. In addition, the dependence of TE and TM modes on the middle waveguide is also weakened.In this design of the device, it is necessary to ensure that the input waveguide and the TM coupling waveguide are phase-matched in the TM mode, but not phase-matched in the TE mode. In the case of the TE coupling waveguide, the principle of phase matching for TE mode is similar. The finite element method is used to calculate the mode field distribution and effective refractive index of silicon waveguides and a hybrid plasmonic waveguide, and then determine the size of each waveguide according to the phase matching conditions, which provides a basis for device modeling and simulation analysis. And the 3D finite difference time domain method is used to study the mode characteristics and optimize the structure of the polarization beam splitter to obtain better performance parameters. The experimental results show that the coupling lengths for TE and TM modes are 4.2 μm and 4.6 μm, respectively, and the polarization conversion efficiency of the modes can reach 94.7% and 95.5%, respectively. It can be seen from the light propagation of the polarization beam splitter that when the TE polarization mode is launched from the input side of the hybrid plasmonic waveguide, it is gradually coupled to the TE coupling port in the coupling region, with scarcely any modes mixing. Similarly, when the TM polarization mode is input into the hybrid plasmonic waveguide, it is finally coupled to the TM coupling port. For the TE mode, the polarization extinction ratio value is −38.9 dB and the insertion loss is −0.5 dB at the wavelength of 1.55 μm. For the wavelength range from 1.48 μm to 1.62 μm, the insertion loss of the TE mode is less than 0.92 dB, and the polarization extinction ratio is lower than −28.3 dB. For the TM mode, the polarization extinction ratio is −34.7dB, and the insertion loss is 0.45 dB at the wavelength of 1.55 μm. In the 140 nm wavelength range centered at 1.55 μm, the insertion loss of the TM mode is less than 0.89 dB, and the polarization extinction ratio is lower than −34.6 dB. The above experimental results mean that the performance of the polarization beam splitter is not sensitive to the wavelength. In addition, the influence of fabrication tolerance of waveguide in polarization beam splitter on device performance is also studied. Within the fabrication tolerance range of waveguides, the insertion loss of the mode is less

than 2.8 dB, and the extinction ratio is lower than －22.5 dB. The results show that the device has high fabrication tolerances. In summary, the polarization beam splitter designed in this paper has a high extinction ratio, low insertion loss, and the coupling length is only 4.6 μm. It has great potential application value in the ultra-small silicon-based optical integrated circuits in the future.

Key words: Integrated optics device; Polarization beam splitter; Finite difference time domain; Optical waveguides; Extinction ratio; Insertion loss

OCIS Codes: 130.3120; 230.1360; 230. 3120; 230. 7370

Foundation item: National Natural Science Foundation of China (Nos.61661025, 62161016)